

# Chiral Skyrmions Interacting with Chiral Flowers

Xichao Zhang,<sup>1,\*</sup> Jing Xia,<sup>2,\*</sup> Oleg A. Tretiakov,<sup>3</sup> Motohiko Ezawa,<sup>4</sup> Guoping Zhao,<sup>5</sup> Yan Zhou,<sup>6</sup>  
Xiaoxi Liu,<sup>2,†</sup> and Masahito Mochizuki<sup>1,‡</sup>

<sup>1</sup>*Department of Applied Physics, Waseda University, Okubo, Shinjuku-ku, Tokyo 169-8555, Japan*

<sup>2</sup>*Department of Electrical and Computer Engineering, Shinshu University, 4-17-1 Wakasato, Nagano 380-8553, Japan*

<sup>3</sup>*School of Physics, The University of New South Wales, Sydney 2052, Australia*

<sup>4</sup>*Department of Applied Physics, The University of Tokyo, 7-3-1 Hongo, Tokyo 113-8656, Japan*

<sup>5</sup>*College of Physics and Electronic Engineering, Sichuan Normal University, Chengdu 610068, China*

<sup>6</sup>*School of Science and Engineering, The Chinese University of Hong Kong, Shenzhen, Guangdong 518172, China*

(Dated: September 19, 2023)

The chiral nature of active matter plays an important role in the dynamics of active matter interacting with chiral structures. Magnetic skyrmions are chiral objects, and their interaction with chiral nanostructures can lead to intriguing phenomena. Here, we explore the dynamics of a thermally activated chiral skyrmion interacting with a chiral flower-like obstacle in a ferromagnetic layer with chiral exchange interactions. The chiralities from different aspects in the studied system give rise to nontrivial random-walk dynamics that may have implications for spintronic applications. We demonstrate that the thermal random walk of chiral skyrmions interacting with chiral flowers could lead to deterministic outcomes that are topology-dependent. It is a spontaneous mesoscopic order-from-disorder phenomenon driven by the thermal fluctuations and topological nature of skyrmions, which exists only in ferromagnetic and ferrimagnetic substrates with chiral flower-like obstacles. The interactions between the skyrmions and chiral flowers at finite temperatures can be utilized to control the skyrmion position and distribution without the application of any external driving force or temperature gradient. The fact that a thermally activated skyrmion could be dynamically coupled to a chiral flower may open a new way for the design of topological sorting devices based on chiral flower-like nanostructures.

**Introduction.**— Chiral skyrmions are versatile topological objects with fixed chirality in magnets with chiral exchange interactions [1–10]. They can be created in magnetic thin films [11], multilayers [12], and bulk nanostructures [13, 14], where they can also be driven into motion by external forces [3–10]. As skyrmions are usually rigid and nonvolatile [3–10, 15], they could be employed as nanoscale information carriers in next-generation information processing applications [16], including data storage [17, 18] and logic computing [19]. Recent studies also suggest that skyrmions can be used as building blocks in future nonconventional applications, including the neuromorphic [20] and quantum computing [21, 22].

The skyrmion dynamics is essential for skyrmionic devices. The dynamics of chiral skyrmions stabilized by chiral exchange interactions [23, 24] in ferromagnets include two aspects, i.e., the motion driven by applied forces [3–10, 16] and the spontaneous diffusion induced by thermal fluctuations [25–49]. For example, a skyrmion driven by the spin-orbit torques may show the skyrmion Hall effect [30, 33, 50, 51], where the skyrmion moves at an angle with respect to the applied current direction. On the other hand, a skyrmion driven by thermal effects may show the Brownian gyromotion [27–29, 31, 32, 34, 38–41, 47], where the skyrmion tends to move in circular trajectories during the random walk. Skyrmions can also be driven into directional motion by thermal gradients [25, 26, 35, 42]. Both the skyrmion Hall effect and skyrmion Brownian diffusion in the ferromagnetic

and ferrimagnetic systems depend on the topological charge carried by the skyrmion (i.e., the skyrmion number), which is defined as  $Q = \frac{1}{4\pi} \int \mathbf{m} \cdot (\frac{\partial \mathbf{m}}{\partial x} \times \frac{\partial \mathbf{m}}{\partial y}) dx dy$  with  $\mathbf{m}$  being the reduced net magnetization [7]. The topology-dependent dynamic behaviors of skyrmions, either spontaneous or forced, are fundamental for practical applications and require precise control in nanostructures.

An important issue in the control and manipulation of skyrmion dynamics in nanostructures is the skyrmion-substrate interactions [9, 52–55]. In active matter systems, the particle-particle and particle-substrate interactions play an important role in the particle dynamics [56, 57]. As nanoscale skyrmions are usually rigid and can show self-motion at finite temperature (i.e., Brownian motion), they can also be treated as a special type of active quasiparticles and interact with the substrate effectively [9, 15, 52–55, 58]. Moreover, the skyrmion-substrate interactions may result in some unique features due to the nontrivial topological nature of skyrmions [9, 15, 52–55, 58].

In 2013, Mijalkov and Volpe demonstrated the possibility that particlelike chiral microswimmers performing circular active Brownian motion can be sorted in a chiral environment formed by using some static obstacle patterns on the substrate [59, 60], where the chirality of circular Brownian motion couples to chiral features present in the environment. As skyrmions also show circular Brownian motion due to their nontrivial topology [27–29, 31, 32, 34, 38–41, 47], it is therefore envisioned that the thermally activated random-walk dynamics of skyrmions may also be modified in a chiral environment due to the skyrmion-substrate interactions, which is the focus of this work.

**Square and Chiral Flower.**— The square and chiral flower-like obstacles considered in this work are schematically de-

\* These authors contributed equally to this work.

† liu@cs.shinshu-u.ac.jp

‡ masa\_mochizuki@waseda.jp

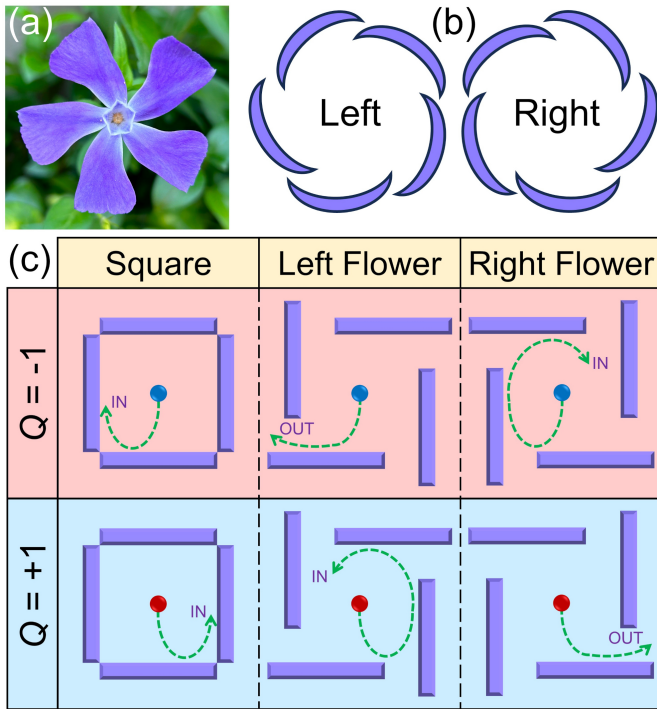


FIG. 1. **A thermally active chiral skyrmion interacting with a chiral flower-like obstacle.** (a) An exemplary chiral flower (*Vinca minor*) found in Shinjuku City by the authors, which shows a fixed left-contort corolla. (b) Diagrams showing the left-right asymmetry in flowers with fixed corolla contortion, i.e., the left-contort and right-contort corollas. (c) Typical outcomes of a chiral skyrmion interacting with a chiral flower or a square: skyrmion confined (i.e., “IN”) and skyrmion escaped (i.e., “OUT”). The outcomes depend on the skyrmion number  $Q$  as well as the left-right asymmetry of the chiral flower. The skyrmions with  $Q = -1$  and  $Q = +1$  are denoted by blue and red dots, respectively.

picted in Fig. 1. A real example of chiral flower is given in Fig. 1(a), which is a left-handed flower showing a fixed left-contort corolla. The chirality of a flower, either left-handed or right-handed [Fig. 1(b)], is an important property of floral symmetry. Some flowers have a contort petal aestivation, which is most pronounced in floral buds and may be less prominent in open flowers [61, 62]. In chiral flowers, two morphs are possible as shown in Fig. 1(b): contorted to the left and contorted to the right [61, 62]. Micro- and nanostructures mimicking chiral flowers may control the dynamics of active chiral matter [56, 57, 59, 60] as well as thermally active chiral skyrmions. In Fig. 1(c), a thermally active skyrmion shows clockwise or counter-clockwise Brownian gyromotion, which depends on the sign of  $Q$ . If a skyrmion is initially placed within a chiral flower, it may escape from or be confined by the chiral flower. The outcome depends on the chirality of the flower and the sign of  $Q$ , which could result in the topological sorting and create an order (sorting)-from-disorder (Brownian motion) phenomenon. However, if a skyrmion is initially placed within a square obstacle, it will be confined by the square.

**Skyrmions Interacting with a Square.**— We first show the

typical Brownian gyromotion of a ferromagnetic skyrmion within a square obstacle, which results in the confinement of the skyrmion [39, 41, 63]. The length, width, and thickness of the ferromagnetic layer equal 256 nm, 256 nm, and 1 nm, respectively. The square pattern is made of four obstacle bars, which are rectangle regions locally modified to have enhanced PMA  $K_o$ . We assume that  $K_o/K = 10$  in order to make sure that the skyrmions cannot penetrate the obstacle boundary [64]. Such a square pattern on the ferromagnetic substrate can, in principle, be fabricated in experiments [41, 65–67]. The width of each obstacle bar is 10 nm, and the distance between two parallel inner edges of the square pattern is 100 nm. The distance between two parallel outer edges is thus 120 nm. The square center overlaps the ferromagnetic layer center, as indicated in Fig. 2(a). Other modeling details and parameters are given in Methods.

Initially, a skyrmion is placed and relaxed at the center of the ferromagnetic layer. We then simulate the thermal random-walk dynamics (i.e., the Brownian motion) of the skyrmion at the temperature of  $T = 150$  K for 500 ns. The trajectories of the skyrmions with  $Q = -1$  and  $Q = +1$  are given in Figs. 2(a) and 2(b), respectively. The skyrmion with  $Q = -1$  shows clockwise Brownian gyromotion [Fig. 2(c)] (see [Supplementary Video 1](#) in Ref. 68), while the skyrmion with  $Q = +1$  shows counter-clockwise Brownian gyromotion [Fig. 2(d)] (see [Supplementary Video 2](#) in Ref. 68). The skyrmions may move along the inner edges of the square and follows the direction of the intrinsic Brownian gyromotion. The confinement leads to a square shape of the overlapped skyrmion position distribution for 500 ns of simulation. The skyrmion motion guided by the square edges is similar to that guided by grain boundaries [38], which may enhance the skyrmion diffusion. The Brownian gyromotion of a skyrmion is a feature of its topological nature, which is due to the Magnus force associated with the net skyrmion number [27–29, 31, 32, 34, 38–41, 47]. We note that the Magnus force is absent in the antiferromagnetic system, where a skyrmion may not show Brownian gyromotion [29, 47].

The time-dependent velocities of the skyrmions with  $Q = -1$  and  $Q = +1$  interacting with the square are given in Fig. 2(e) and 2(f), respectively. The velocity is randomly fluctuating with time and the mean value for the skyrmion with  $Q = -1$  equals  $0.60 \text{ m s}^{-1}$ , which is almost the same with that of the skyrmion with  $Q = +1$  ( $0.68 \text{ m s}^{-1}$ ). The clockwise and counter-clockwise Brownian gyromotion can also be seen from the time-dependent skyrmion Hall angle defined as  $\theta_{\text{SkHE}} = \arctan(v_y/v_x)$  with  $v_x$  and  $v_y$  being the  $x$  and  $y$  components of the skyrmion velocity, respectively. In Fig. 2(g), the clockwise skyrmion motion is indicated by the continuous decrease and sharp increase of  $\theta_{\text{SkHE}}(t)$ . The counter-clockwise skyrmion motion is indicated by the continuous increase and sharp decrease of  $\theta_{\text{SkHE}}(t)$  [Fig. 2(h)]. The radius of the skyrmion with  $Q = \pm 1$  interacting with the square is also fluctuating with time, and its mean value equals 7 nm during 500 ns of simulation [Fig. 2(i)].

**Skyrmions Interacting with a Chiral Flower.**— Here we demonstrate typical two outcomes of a thermally active skyrmion with  $Q = \pm 1$  interacting with a left- or right-handed

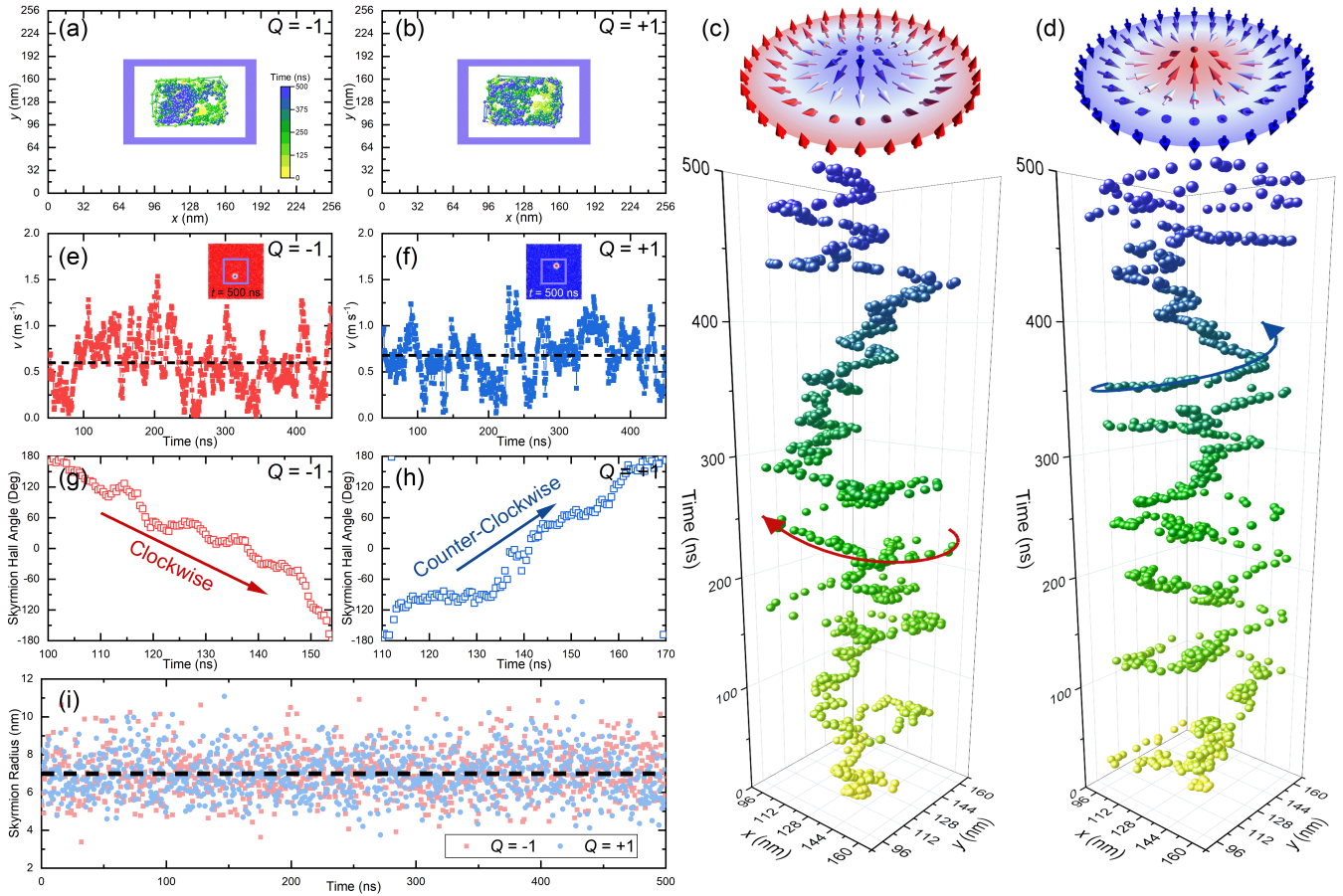


**FIG. 2. A thermally active skyrmion confined by a square obstacle.** Typical trajectories of (a) a skyrmion with  $Q = -1$  and (b) a skyrmion with  $Q = +1$  confined by a square are given. Three-dimensional illustrations show the time-dependent skyrmion position and the skyrmion texture with (c)  $Q = -1$  or (d)  $Q = +1$ . The skyrmions with  $Q = -1$  and  $Q = +1$  show clockwise and counter-clockwise circular motion along the inner edges of the square obstacle, respectively. Time-dependent velocities  $v$  of the skyrmions with (e)  $Q = -1$  and (f)  $Q = +1$  are given. Time-dependent skyrmion Hall angles of the skyrmions with (g)  $Q = -1$  and (h)  $Q = +1$  are also shown for selected time ranges, indicating the clockwise and counter-clockwise circular motion, respectively. (i) Time-dependent skyrmion radius. The skyrmion dynamics is simulated at  $T = 150$  K for 500 ns with a time step of 0.5 ns.

flower-like obstacle pattern. The chiral flower pattern is made of four obstacle bars, which are rectangle regions with enhanced PMA  $K_o/K = 10$ . The width and length of each obstacle bar are equal to 10 nm and 120 nm, respectively. The distance between two parallel inner edges of the obstacle bars is 100 nm. The opening width between two orthogonal obstacle bars is set to 30 nm. The chiral flower center overlaps the ferromagnetic layer center, as shown in Fig. 3(a). The opening width should be wider but not much wider than the skyrmion diameter, and the area within the chiral flower should not be too large. Otherwise, the skyrmion may not interact with the chiral flower in an effective way depending on its diffusion at a given temperature.

A skyrmion is initially placed and relaxed at the ferromagnetic layer center. We then simulate the thermal random-walk dynamics of the skyrmion at a given temperature for 500 ns. We first show typical desired outcome of the skyrmion with  $Q = \pm 1$  interacting with a left- or right-handed flower at  $T = 150$  K in Figs. 3(a)-3(d). The skyrmion with  $Q =$

$-1$  shows the clockwise Brownian gyromotion [Figs. 3(e) and 3(g)]. Consequently, its interactions with the left-handed [Fig. 3(a)] and right-handed [Fig. 3(c)] chiral flowers lead to the outcomes “OUT” and “IN”, respectively, within 500 ns of simulation (see [Supplementary Videos 3 and 4](#) in Ref. 68). The skyrmions with  $Q = +1$  showing the counter-clockwise Brownian gyromotion [Figs. 3(f) and 3(h)] and interacting with the left-handed [Fig. 3(b)] and right-handed [Fig. 3(d)] chiral flowers show the outcomes “IN” and “OUT”, respectively (see [Supplementary Videos 5 and 6](#) in Ref. 68). The desired and expected outcomes for the four skyrmion-flower configurations are summarized schematically in Fig. 1(c). The time-dependent velocity and skyrmion radius during the skyrmion-flower interaction are given in [Supplementary Fig. 1](#) [68].

The desired outcome may be achieved when the skyrmion interacts effectively with the chiral flower for enough long time. However, as a skyrmion has a certain lifetime at finite temperature, it may be collapsed before or after the achieve-



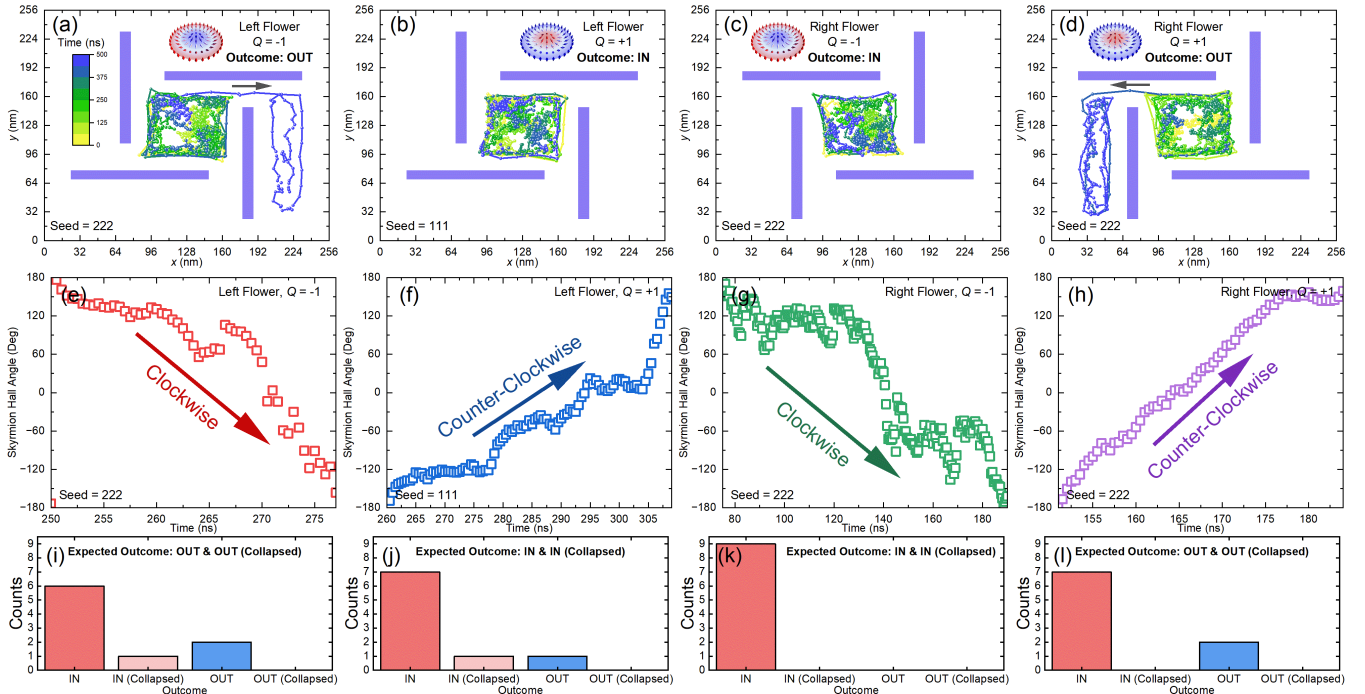


FIG. 3. **A thermally active skyrmion interacting with a left-handed or right-handed flower.** (a) Typical trajectory of a skyrmion with  $Q = -1$  interacting with a left-handed flower. The skyrmion escapes from the left-handed flower due to its clockwise Brownian gyromotion, i.e, the outcome is “OUT”. (b) Typical trajectory of a skyrmion with  $Q = +1$  interacting with a left-handed flower. The skyrmion is confined by the left-handed flower due to its counter-clockwise Brownian gyromotion, i.e, the outcome is “IN”. (c) Typical trajectory of a skyrmion with  $Q = -1$  interacting with a right-handed flower. The skyrmion is confined by the right-handed flower due to its clockwise Brownian gyromotion, i.e, the outcome is “IN”. (d) Typical trajectory of a skyrmion with  $Q = +1$  interacting with a right-handed flower. The skyrmion escapes from the right-handed flower due to its counter-clockwise Brownian gyromotion, i.e, the outcome is “OUT”. (e)–(h) Time-dependent skyrmion Hall angles for selected time ranges, corresponding to (a)–(b), respectively. (i)–(l) The outcome counts for a skyrmion with  $Q = \pm 1$  interacting with a left- or right-handed flower. Nine simulations are done with different random seeds for each skyrmion-flower configuration. The skyrmion dynamics is simulated at  $T = 150$  K for 500 ns with a time step of 0.5 ns.

ment of the desired outcome. We perform nine simulations with different random seeds and summarize the outcome for each temperature and skyrmion-flower configuration. For the skyrmion with  $Q = -1$  interacting with a left-handed flower, we obtain two events of desired outcome in nine simulations [Fig. 3(i)]. For the skyrmion with  $Q = +1$  interacting with a left-handed flower, we obtain eight events of desired outcome [Fig. 3(j)], including one case where the skyrmion collapses within the chiral flower. We also note that an unexpected “OUT” event happens, which may due to the fact that the skyrmion size is transiently much smaller than the opening width when it moves to an exit of the left-handed flower (see [Supplementary Video 7](#) in Ref. 68). Such a situation may be avoided by slightly reducing the opening width or increasing the skyrmion size. For the skyrmion with  $Q = -1$  interacting with a right-handed flower, we obtain nine events of desired outcome [Fig. 3(k)]. For the skyrmion with  $Q = +1$  interacting with a right-handed flower, we obtain two events of desired outcome [Fig. 3(l)].

In Fig. 4, we further show that the probability of achieving the desired and expected outcome for the skyrmion-flower interaction depends on the temperature. When the temperature is too low [Fig. 4(a);  $T = 100$  K], the skyrmion diffusion is

weak and it cannot interact with the chiral flower effectively. In such a case, we obtain nine “IN” events in nine simulations for the skyrmions with  $Q = \pm 1$  within a right-handed flower. When  $T = 150$  K [Fig. 4(b)], we obtain nine desired “IN” events for the skyrmion with  $Q = -1$  interacting a right-handed flower, and two desired “OUT” events for the skyrmion with  $Q = +1$  interacting with a right-handed flower. When  $T = 180$  K [Fig. 4(c)], we obtain nine desired “IN” events for the skyrmion with  $Q = -1$  interacting a right-handed flower, and three desired “OUT” events for the skyrmion with  $Q = +1$  interacting with a right-handed flower. It suggests that the skyrmion-flower interaction could be more effective due to more active skyrmion at elevated temperature. However, when the temperature is too high [Fig. 4(d);  $T = 200$  K], the thermal fluctuations may result in the collapse of the skyrmion in more simulations due to significantly reduced skyrmion lifetime. The mean skyrmion size may also increase with the temperature. Therefore, the skyrmion may not interact with the chiral flower effectively when the temperature is too high.

**Conclusion.**— We have studied the thermal random-walk dynamics of a ferromagnetic skyrmion in a chiral environment, where the interactions between skyrmions and chiral

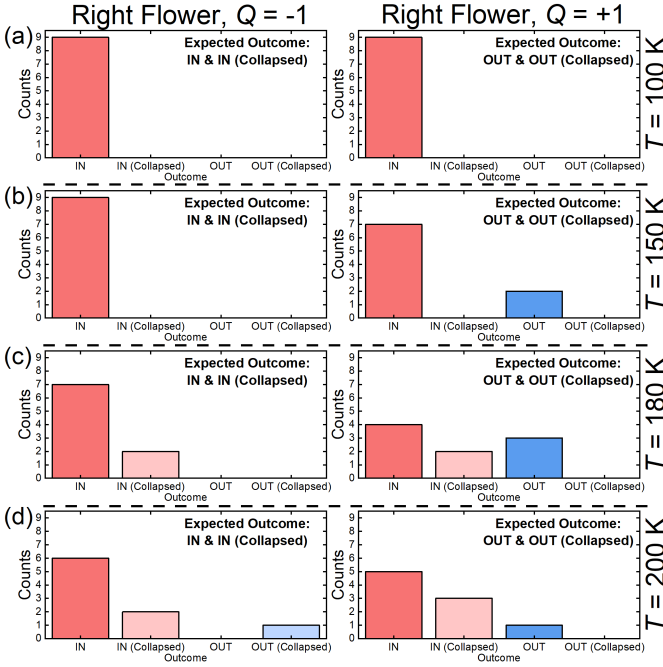


FIG. 4. **The outcome counts for a skyrmion interacting with a right-handed flower at different temperatures.** A skyrmion with  $Q = \pm 1$  interacting with a right-handed flower at (a)  $T = 100$  K, (b)  $T = 150$  K, (c)  $T = 180$  K, and (d)  $T = 200$  K. Nine simulations are done with different random seeds for each temperature. The skyrmion dynamics is simulated for 500 ns with a time step of 0.5 ns.

obstacles (i.e., the chiral flowers) could lead to the topology-dependent spontaneous sorting of skyrmions. The position of a skyrmion can be manipulated by using a simple chiral flower-like obstacle pattern at finite temperature in the absence of an external drive. Our results reveal unique thermal dynamics of chiral topological spin textures interacting with chiral structures. Our results also suggest that it is possible to build a topological sorting device based on chiral flower-like structures, in which skyrmions with opposite signs of topological charges could show different dynamic outcomes.

**Methods.**— The simulations are performed by using the micromagnetic simulator MUMAX<sup>3</sup> [69, 70] on a commercial graphics processing unit NVIDIA GeForce RTX 3080. The magnetization dynamics at finite temperature is governed by the stochastic Landau-Lifshitz-Gilbert (LLG) equation [69, 70],

$$\partial_t \mathbf{m} = -\gamma_0 \mathbf{m} \times (\mathbf{h}_{\text{eff}} + \mathbf{h}_f) + \alpha (\mathbf{m} \times \partial_t \mathbf{m}), \quad (1)$$

where  $\mathbf{m} = \mathbf{M}/M_S = 1$  is the reduced magnetization,  $M_S$  is the saturation magnetization,  $t$  is the time,  $\gamma_0$  is the absolute gyromagnetic ratio,  $\alpha$  is the Gilbert damping parameter,  $\mathbf{h}_{\text{eff}} = -\frac{1}{\mu_0 M_S} \cdot \frac{\delta \varepsilon}{\delta \mathbf{m}}$  is the effective field with  $\mu_0$  and  $\varepsilon$  being the vacuum permeability constant and average energy density, respectively.  $\mathbf{h}_f$  is a thermal fluctuating field satisfy-

ing [69, 70]

$$\begin{aligned} \langle h_i(\mathbf{x}, t) \rangle &= 0, \\ \langle h_i(\mathbf{x}, t) h_j(\mathbf{x}', t') \rangle &= \frac{2\alpha k_B T}{M_S \gamma_0 \mu_0 V} \delta_{ij} \delta(\mathbf{x} - \mathbf{x}') \delta(t - t'), \end{aligned} \quad (2)$$

where  $i$  and  $j$  are Cartesian components,  $k_B$  is the Boltzmann constant,  $T$  is the temperature, and  $V$  is the volume of a single mesh cell.  $\delta_{ij}$  and  $\delta(\dots)$  denote the Kronecker and Dirac delta symbols, respectively. The energy terms considered in the model include the ferromagnetic exchange energy, interface-induced chiral exchange energy, perpendicular magnetic anisotropy (PMA) energy, and demagnetization energy. Thus, the average energy density is given as [69, 70]

$$\begin{aligned} \varepsilon &= A (\nabla \mathbf{m})^2 + D [m_z (\mathbf{m} \cdot \nabla) - (\nabla \cdot \mathbf{m}) m_z] \\ &\quad - K (\mathbf{n} \cdot \mathbf{m})^2 - \frac{M_S}{2} (\mathbf{m} \cdot \mathbf{B}_d), \end{aligned} \quad (3)$$

where  $A$ ,  $D$ , and  $K$  are the ferromagnetic exchange, DM interaction, and PMA constants, respectively.  $\mathbf{B}_d$  is the demagnetization field.  $\mathbf{n}$  is the unit surface normal vector.  $m_z$  is the out-of-plane component of  $\mathbf{m}$ . The default magnetic parameters are 17–19, and 64:  $\gamma_0 = 2.211 \times 10^5 \text{ m A}^{-1} \text{ s}^{-1}$ ,  $\alpha = 0.1$ ,  $M_S = 580 \text{ kA m}^{-1}$ ,  $A = 15 \text{ pJ m}^{-1}$ ,  $K = 0.8 \text{ MJ m}^{-3}$ , and  $D = 3 \text{ mJ m}^{-2}$ . The mesh size is  $2 \times 2 \times 1 \text{ nm}^3$ , which ensures good computational accuracy and efficiency. The finite-temperature simulation is performed with a fixed time step of 10 fs and a given random seed.

**Data availability.** The data that support the findings of this study are available from the corresponding authors upon reasonable request.

**Code availability.** The simulator MUMAX<sup>3</sup> used in this work is publicly accessible at <http://mumax.github.io/index.html>.

## ACKNOWLEDGMENTS

**Acknowledgments.**— X.Z. and M.M. acknowledge support by CREST, the Japan Science and Technology Agency (Grant No. JPMJCR20T1). M.M. also acknowledges support by the Grants-in-Aid for Scientific Research from JSPS KAKENHI (Grant No. JP20H00337). J.X. was a JSPS International Research Fellow supported by JSPS KAKENHI (Grant No. JP22F22061). O.A.T. acknowledges support by the Australian Research Council (Grant No. DP200101027), the Cooperative Research Project Program at the Research Institute of Electrical Communication, Tohoku University (Japan), and by the NCMAS grant. M.E. acknowledges support by CREST, JST (Grant No. JPMJCR20T2). G.Z. acknowledges support by the National Natural Science Foundation of China (Grants No. 51771127, No. 51571126, and No. 51772004), and Central Government Funds of Guiding Local Scientific and Technological Development for Sichuan Province (Grant No. 2021ZYD0025). Y.Z. acknowledges support by the Guangdong Basic and Applied Basic Research

Foundation (Grant No. 2021B1515120047), the Guangdong Special Support Project (Grant No. 2019BT02X030), the Shenzhen Fundamental Research Fund (Grant No. JCYJ20210324120213037), the Shenzhen Peacock Group Plan (Grant No. KQTD20180413181702403), the Pearl River

Recruitment Program of Talents (Grant No. 2017GC010293), and the National Natural Science Foundation of China (Grants No. 11974298 and No. 12374123). X.L. acknowledges support by the Grants-in-Aid for Scientific Research from JSPS KAKENHI (Grants No. JP20F20363, No. JP21H01364, No. JP21K18872, and No. JP22F22061).

- 
- [1] A. N. Bogdanov and D. A. Yablonskii, *Sov. Phys. JETP* **68**, 101 (1989).
- [2] U. K. Röbber, A. N. Bogdanov, and C. Pfeleiderer, *Nature* **442**, 797 (2006).
- [3] N. Nagaosa and Y. Tokura, *Nat. Nanotech.* **8**, 899 (2013).
- [4] M. Mochizuki and S. Seki, *J. Phys.: Condens. Matter* **27**, 503001 (2015).
- [5] A. Fert, N. Reyren, and V. Cros, *Nat. Rev. Mater.* **2**, 17031 (2017).
- [6] K. Everschor-Sitte, J. Masell, R. M. Reeve, and M. Kläui, *J. Appl. Phys.* **124**, 240901 (2018).
- [7] X. Zhang, Y. Zhou, K. M. Song, T.-E. Park, J. Xia, M. Ezawa, X. Liu, W. Zhao, G. Zhao, and S. Woo, *J. Phys. Condens. Matter* **32**, 143001 (2020).
- [8] B. Göbel, I. Mertig, and O. A. Tretiakov, *Phys. Rep.* **895**, 1 (2021).
- [9] C. Reichhardt, C. J. O. Reichhardt, and M. V. Milosevic, *Rev. Mod. Phys.* **94**, 035005 (2022).
- [10] N. Del-Valle, J. Castell-Queralt, L. González-Gómez, and C. Navau, *APL Mater.* **10**, 010702 (2022).
- [11] N. Romming, C. Hanneken, M. Menzel, J. E. Bickel, B. Wolter, K. von Bergmann, A. Kubetzka, and R. Wiesendanger, *Science* **341**, 636 (2013).
- [12] W. Jiang, P. Upadhyaya, W. Zhang, G. Yu, M. B. Jungfleisch, F. Y. Fradin, J. E. Pearson, Y. Tserkovnyak, K. L. Wang, O. Heinonen, S. G. E. te Velthuis, and A. Hoffmann, *Science* **349**, 283 (2015).
- [13] S. Mühlbauer, B. Binz, F. Jonietz, C. Pfeleiderer, A. Rosch, A. Neubauer, R. Georgii, and P. Böni, *Science* **323**, 915 (2009).
- [14] X. Z. Yu, Y. Onose, N. Kanazawa, J. H. Park, J. H. Han, Y. Matsui, N. Nagaosa, and Y. Tokura, *Nature* **465**, 901 (2010).
- [15] S.-Z. Lin, C. Reichhardt, C. D. Batista, and A. Saxena, *Phys. Rev. B* **87**, 214419 (2013).
- [16] W. Kang, Y. Huang, X. Zhang, Y. Zhou, and W. Zhao, *Proc. IEEE* **104**, 2040 (2016).
- [17] J. Sampaio, V. Cros, S. Rohart, A. Thiaville, and A. Fert, *Nat. Nanotechnol.* **8**, 839 (2013).
- [18] R. Tomasello, E. Martinez, R. Zivieri, L. Torres, M. Carpentieri, and G. Finocchio, *Sci. Rep.* **4**, 6784 (2014).
- [19] X. Zhang, M. Ezawa, and Y. Zhou, *Sci. Rep.* **5**, 9400 (2015).
- [20] K. M. Song, J.-S. Jeong, B. Pan, X. Zhang, J. Xia, S. Cha, T.-E. Park, K. Kim, S. Finizio, J. Raabe, J. Chang, Y. Zhou, W. Zhao, W. Kang, H. Ju, and S. Woo, *Nat. Electron.* **3**, 148 (2020).
- [21] C. Psaroudaki and C. Panagopoulos, *Phys. Rev. Lett.* **127**, 067201 (2021).
- [22] J. Xia, X. Zhang, X. Liu, Y. Zhou, and M. Ezawa, *Phys. Rev. Lett.* **130**, 106701 (2023).
- [23] I. Dzyaloshinskii, *J. Phys. Chem. Solids* **4**, 241 (1958).
- [24] T. Moriya, *Phys. Rev.* **120**, 91 (1960).
- [25] L. Kong and J. Zang, *Phys. Rev. Lett.* **111**, 067203 (2013).
- [26] S. Z. Lin, C. D. Batista, C. Reichhardt, and A. Saxena, *Phys. Rev. Lett.* **112**, 187203 (2014).
- [27] R. E. Troncoso and A. S. Núñez, *Ann. Phys.* **351**, 850 (2014).
- [28] C. Schütte, J. Iwasaki, A. Rosch, and N. Nagaosa, *Phys. Rev. B* **90**, 174434 (2014).
- [29] J. Barker and O. A. Tretiakov, *Phys. Rev. Lett.* **116**, 147203 (2016).
- [30] C. Reichhardt and C. J. O. Reichhardt, *New J. Phys.* **18**, 095005 (2016).
- [31] J. Miltat, S. Rohart, and A. Thiaville, *Phys. Rev. B* **97**, 214426 (2018).
- [32] T. Nozaki, Y. Jibiki, M. Goto, E. Tamura, T. Nozaki, H. Kubota, A. Fukushima, S. Yuasa, and Y. Suzuki, *Appl. Phys. Lett.* **114**, 012402 (2019).
- [33] C. Reichhardt and C. J. O. Reichhardt, *J. Phys.: Condens. Matter* **31**, 07LT01 (2019).
- [34] L. Zhao, Z. Wang, X. Zhang, X. Liang, J. Xia, K. Wu, H. A. Zhou, Y. Dong, G. Yu, K. L. Wang, X. Liu, Y. Zhou, and W. Jiang, *Phys. Rev. Lett.* **125**, 027206 (2020).
- [35] Z. Wang, M. Guo, H. A. Zhou, L. Zhao, T. Xu, R. Tomasello, H. Bai, Y. Dong, S. G. Je, W. Chao, H. S. Han, S. Lee, K. S. Lee, Y. Yao, W. Han, C. Song, H. Wu, M. Carpentieri, G. Finocchio, M. Y. Im, S. Z. Lin, and W. Jiang, *Nat. Electron.* **3**, 672 (2020).
- [36] Y. Yao, X. Chen, W. Kang, Y. Zhang, and W. Zhao, *IEEE Trans. Electron Devices* **67**, 2553 (2020).
- [37] K. Y. Jing, C. Wang, and X. R. Wang, *Phys. Rev. B* **103**, 174430 (2021).
- [38] Y. Zhou, R. Mansell, T. Ala-Nissila, and S. van Dijken, *Phys. Rev. B* **104**, 144417 (2021).
- [39] S. Miki, Y. Jibiki, E. Tamura, M. Goto, M. Oogane, J. Cho, R. Ishikawa, H. Nomura, and Y. Suzuki, *J. Phys. Soc. Jpn.* **90**, 083601 (2021).
- [40] Y. Suzuki, S. Miki, Y. Imai, and E. Tamura, *Phys. Lett. A* **413**, 127603 (2021).
- [41] R. Ishikawa, M. Goto, H. Nomura, and Y. Suzuki, *Appl. Phys. Lett.* **119**, 072402 (2021).
- [42] X. Yu, F. Kagawa, S. Seki, M. Kubota, J. Masell, F. S. Yasin, K. Nakajima, M. Nakamura, M. Kawasaki, N. Nagaosa, and Y. Tokura, *Nat. Commun.* **12**, 5079 (2021).
- [43] C. Song, N. Kerber, J. Rothörl, Y. Ge, K. Raab, B. Seng, M. A. Brems, F. Dittrich, R. M. Reeve, J. Wang, Q. Liu, P. Virnau, and M. Kläui, *Adv. Funct. Mater.* **31**, 2010739 (2021).
- [44] N. Kerber, M. Weißenhofer, K. Raab, K. Litzius, J. Zázvorka, U. Nowak, and M. Kläui, *Phys. Rev. Applied* **15**, 044029 (2021).
- [45] L. Kong, X. Chen, W. Wang, D. Song, and H. Du, *Phys. Rev. B* **104**, 214407 (2021).
- [46] M. Weißenhofer, L. Rózsa, and U. Nowak, *Phys. Rev. Lett.* **127**, 047203 (2021).
- [47] M. Weißenhofer and U. Nowak, *Phys. Rev. B* **107**, 064423 (2023).
- [48] R. Gruber, M. A. Brems, J. Rothörl, T. Sparmann, M. Schmitt, I. Kononenko, F. Kammerbauer, M.-A. Syskaki, O. Farago, P. Virnau, and M. Kläui, *Adv. Mater.* **35**, 2208922 (2023).
- [49] T. Dohi, M. Weißenhofer, N. Kerber, F. Kammerbauer, Y. Ge, K. Raab, J. Zázvorka, M.-A. Syskaki, A. Shahee, M. Ruhwedel,

- T. Böttcher, P. Pirro, G. Jakob, U. Nowak, and M. Kläui, *Nat. Commun.* **14**, 5424 (2023).
- [50] W. Jiang, X. Zhang, G. Yu, W. Zhang, X. Wang, M. Benjamin Jungfleisch, J. E. Pearson, X. Cheng, O. Heinonen, K. L. Wang, Y. Zhou, A. Hoffmann, and S. G. E. te Velthuis, *Nat. Phys.* **13**, 162 (2017).
- [51] K. Litzius, I. Lemesch, B. Kruger, P. Bassirian, L. Caretta, K. Richter, F. Buttner, K. Sato, O. A. Tretiakov, J. Forster, R. M. Reeve, M. Weigand, I. Bykova, H. Stoll, G. Schutz, G. S. D. Beach, and M. Kläui, *Nat. Phys.* **13**, 170 (2017).
- [52] C. Reichhardt, D. Ray, and C. J. O. Reichhardt, *Phys. Rev. B* **91**, 104426 (2015).
- [53] C. Reichhardt, D. Ray, and C. J. O. Reichhardt, *New J. Phys.* **17**, 073034 (2015).
- [54] C. Reichhardt and C. J. O. Reichhardt, *Phys. Rev. B* **99**, 104418 (2019).
- [55] N. P. Vizarim, C. Reichhardt, C. J. O. Reichhardt, and P. A. Venegas, *New J. Phys.* **22**, 053025 (2020).
- [56] C. Bechinger, R. Di Leonardo, H. Löwen, C. Reichhardt, G. Volpe, and G. Volpe, *Rev. Mod. Phys.* **88**, 045006 (2016).
- [57] C. J. O. Reichhardt and C. Reichhardt, *Annu. Rev. Condens. Matter Phys.* **8**, 51 (2017).
- [58] Z.-Y. Li, D.-Q. Zhang, S.-Z. Lin, W. T. Gozdz, and B. Li, *Soft Matter* **18**, 7348 (2022).
- [59] M. Mijalkov and G. Volpe, *Soft Matter* **9**, 6376 (2013).
- [60] G. Volpe, S. Gigan, and G. Volpe, *Am. J. Phys.* **82**, 659 (2014).
- [61] P. K. Endress, *Int. J. Plant Sci.* **160**, S3 (1999).
- [62] P. K. Endress, *Curr. Opin. Plant Biol.* **4**, 86 (2001).
- [63] A. Monteil, C. B. Muratov, T. M. Simon, and V. V. Slastikov, *arXiv:2208.00058* (2022).
- [64] X. Zhang, J. Xia, and X. Liu, *Phys. Rev. B* **106**, 094418 (2022).
- [65] R. Juge, K. Bairagi, K. G. Rana, J. Vogel, M. Sall, D. Mailly, V. T. Pham, Q. Zhang, N. Sisodia, M. Foerster, L. Aballe, M. Belmeguenai, Y. Roussigné, S. Auffret, L. D. Buda-Prejbeanu, G. Gaudin, D. Ravelosona, and O. Boulle, *Nano Lett.* **21**, 2989 (2021).
- [66] K. Ohara, X. Zhang, Y. Chen, Z. Wei, Y. Ma, J. Xia, Y. Zhou, and X. Liu, *Nano Lett.* **21**, 4320 (2021).
- [67] X. Zhang, J. Xia, K. Shirai, H. Fujiwara, O. A. Tretiakov, M. Ezawa, Y. Zhou, and X. Liu, *Commun. Phys.* **4**, 255 (2021).
- [68] See Supplemental Material at [URL] for supplementary figures and videos about the thermal random walk dynamics of chiral skyrmions interacting with chiral flowers.
- [69] A. Vansteenkiste, J. Leliaert, M. Dvornik, M. Helsen, F. Garcia-Sanchez, and B. V. Waeyenberge, *AIP Adv.* **4**, 107133 (2014).
- [70] J. Leliaert, M. Dvornik, J. Mulkers, J. De Clercq, M. V. Milošević, and B. Van Waeyenberge, *J. Phys. D: Appl. Phys.* **51**, 123002 (2018).

### Author contributions

X.Z., M.M. and X.L. conceived the idea. X.L. and M.M. coordinated the project. X.Z. and J.X. performed the numerical simulation and the theoretical analysis. X.Z. and J.X. drafted the manuscript and revised it with input from O.A.T., M.E., G.Z., Y.Z., X.L. and M.M. All authors discussed the results and reviewed the manuscript. X.Z. and J.X. contributed equally to this work.

### Competing interests

The authors declare no competing financial interests.